Relativistic, correlation, and polarization effects in two-photon photoionization of Xe

B. M. Lagutin and I. D. Petrov
Rostov State University of Transport Communications, 344038 Rostov-on-Don, Russia

V. L. Sukhorukov
Institute of Physics, Southern Federal University, 344090 Rostov-on-Don, Russia

Ph. V. Demekhin, A. Knie, and A. Ehresmann
Institute of Physics and Center for Interdisciplinary Nanostructure Science and Technology (CINSaT), University Kassel, D-34132, Kassel, Germany

(Received 7 April 2017; published 19 June 2017)

Two-photon ionization of xenon was investigated theoretically for exciting-photon energies from 6.7 to 11.5 eV, which results in the ionization of Xe between $5p_{1/2}$ (13.43 eV) and $5s$ (23.40 eV) thresholds. We describe the extension of a previously developed computational technique for the inclusion of relativistic effects to calculate energies of intermediate resonance state and cross sections for two-photon ionization. Reasonable consistency of cross sections calculated in length and velocity form was obtained only after considering many-electron correlations. Agreement between calculated and measured resonance energies is found when core polarization was additionally included in the calculations. The presently computed two-photon photoionization cross sections of Xe are compared with Ar cross sections in our previous work. Photoelectron angular distribution parameters calculated here indicate that intermediated resonances strongly influence photoelectron angular distribution of Xe.

DOI: 10.1103/PhysRevA.95.063414

I. INTRODUCTION

Recent developments of free-electron laser sources [1–4] upsurged interest in the detailed understanding of multiphoton processes. In contrast to the already well-investigated two- or multiphoton processes of conventional laboratory laser sources at a few defined photon energies, photon energies of free-electron lasers can, in principle, be tuned over a large energy range. This enables the determination of photoionization cross sections and electron angular distributions over a wide photon energy range. In this way data sets will be created serving as benchmarks to test theoretical models.

On the other hand, the present state of the theory of multiphoton processes lags a little behind the experimental demands. As an example of this situation we mention multiphoton multiple ionization of Xe [5] which was interpreted on the basis of the scaling techniques [6,7], so far. Therefore, it is desirable to have the technique which allows one to take into account many-electron effects in the description of the initial and final states as well as in computing transition amplitudes. The relativistic effects in calculation of multiphoton processes in heavy atoms, especially if the spherical shells are involved, need also to be included.

In the present work we continue to develop a description for two-photon photoionization, based on our previous work [8], where a method has been developed to calculate a generalized two-photon ionization cross section (G2PICS [9]) with taking into account many-electron correlations in nonrelativistic approximation. In the present paper we extend the approach by including relativistic effects using accumulated earlier experience in calculation of the single-photon ionization of atoms within the frames of the configuration interaction Pauli-Fock approach with core polarization (CIPFCP) [10].

The challenge of investigating theoretically the G2PICS of Xe lasts now for more than 30 years. McGuire [11] has calculated the G2PICS of noble-gas atoms applying the Green's function technique and straight-line approximation of the nonrelativistic Herman-Skillman potential [12]. Gangopadhyay *et al.* [13] applied multichannel quantum-defect theory (MQDT) to study theoretically two- and three-photon ionization of atomic Xe in the energy range between the $5p_{3/2}$ and $5p_{1/2}$ thresholds as well as slightly above the $5p_{1/2}$ threshold. The values of the MQDT parameters were taken from the experiment. Angular distribution of photoelectrons has also been computed at certain photon energies.

L'Huillier and Wendin [14] improved the accuracy of the $5s$ and $5p$ two-photon ionization calculation of Xe using a nonrelativistic Hartree-Fock single-electron basis in LS coupling. These authors studied the influence of different many-electron correlations on the computed G2PICS in detail. However, an important intermediate-state shake-up correlation was not considered. Later, Pan *et al.* [15] showed that, namely, this correlation provided close agreement between the cross sections of the $3p$ two-photon ionization of Ar, calculated in the length (L) and velocity (V) forms of the dipole transition operator.

Fink and Johnson [16] took into account relativistic effects in computing the G2PICS of the outer shells of the rare-gas atoms Ne, Ar, Kr, and Xe using a time-dependent Dirac-Fock (TDDF) method which was noted to be closely related to the relativistic random-phase approximation (RRPA). The cross sections were obtained in the length form at energies near the first intermediate-state resonance. Both photoionization by linearly and circularly polarized exciting photons were investigated. The calculation of the G2PICS by this method, however, diverged at the vicinity of resonances.

So far, none of the different previous calculations was able to simultaneously account for relativistic effects, many-electron correlations (including shake-up interaction), and the effect of core polarization by the outgoing photoelectron. The core polarization (CP), in particular, was found to be important in the case of the $3p$ G2PICS of Ar [8]. Its inclusion resulted in a 17% increase of the Ar $3p$ G2PICS at the threshold and provided very good agreement of the computed and measured energies of the intermediate resonances. Therefore, here, we present a method where CP and many-electron effects are considered in a relativistic approach.

As an object of study, we chose the two-photon ionization of the $5p$ shell of Xe because both relativistic and many-electron effects are expected to have substantial impact on this process. Relatively small exciting-photon energies allow us to avoid problems concerning the above threshold ionization [17].

The paper is organized as follows. In Sec. II we describe the relativistic extension of the computation method including the correlation function (CF) technique and details of the used basis atomic orbitals (AOs) (Sec. II C). Section III presents the results of the calculation of Xe $5p$ G2PICS. We discuss the differences between the computed $3p$ Ar G2PICS and $5p$ Xe G2PICS in Sec. III A. The influence of relativistic and polarization effects on the calculated energies of the intermediate resonances is investigated in Sec. III B. Presently computed G2PICSs are compared with other theoretical data in Sec. III D. The calculated angular distribution of photoelectrons is presented in Sec. IV. We conclude with a brief summary in Sec. V.

II. THEORY

In order to compute the two-photon ionization of Xe we used the jj coupling scheme:

$$\mathrm{Xe}\,5p^6(J_0=0)+2\gamma \rightarrow \mathrm{Xe}^+5p^5_{j_c}\varepsilon\ell j(J) \qquad (J=0,2), \tag{1}$$

where j_c is the total momentum of the $5p^5$ ionic core; ℓ and j are orbital and total angular momentum of the photoelectron, respectively; and J_0 and J are total angular momenta of the initial and final state, respectively. The jj coupling was chosen in the present work instead of the LS coupling used in [8] because of the larger splitting $E^{(i)}_{5p_{1/2}}-E^{(i)}_{5p_{3/2}}=1.31$ eV in Xe as compared to $E^{(i)}_{3p_{1/2}}-E^{(i)}_{3p_{3/2}}=0.18$ eV in Ar (see data [18]). Thus, the following eight channels were included in the calculation: $5p^5_{3/2}\varepsilon p_{3/2}(J=0,2)$, $5p^5_{3/2}\varepsilon p_{1/2}(J=2)$, $5p^5_{3/2}\varepsilon f_{5/2}(J=2)$, $5p^5_{3/2}\varepsilon f_{7/2}(J=2)$, $5p^5_{1/2}\varepsilon p_{1/2}(J=0)$, $5p^5_{1/2}\varepsilon p_{3/2}(J=2)$, and $5p^5_{1/2}\varepsilon f_{5/2}(J=2)$.

In order to describe the two-photon ionization quantitatively we used, as in our previous work [8], the generalized photoionization cross section (G2PICS) which has the dimension cm^4 s and is the property of an atom (i.e., it is independent of the strength of the exciting radiation [9]).The total G2PICS $\sigma_q(\omega)$ is expressed as a sum of partial cross sections $\sigma_q(j_c,\ell,j,J,\omega)$:

$$\sigma_q(\omega)=\sum_{j_c,\ell,j,J}\sigma_q(j_c,\ell,j,J,\omega), \tag{2}$$

where $q=0$ and ±1 notes the linearly polarized and the circularly polarized incident radiation, respectively. Partial G2PICS we define as

$$\sigma_q(j_c,\ell,j,J,\omega)=\frac{8\pi^3\alpha a_0^5}{c}\omega^{\pm2}|T_{q,\omega}(j_c,\ell,j,J)|^2, \tag{3}$$

where $\alpha=1/137.036$ is the fine-structure constant; $a_0=5.291\,77\times10^{-9}$ cm is the Bohr radius; $c=2.997\,92\times10^{10}$ cm/s is the light velocity in vacuum; ω is the exciting-photon energy (in atomic units) of one of the two photons, assuming the same energy for the other photon; and "+" and "−" correspond to the length and velocity gauges of the electrical dipole operator, respectively.

In the lowest order of perturbation theory (LOPT), the two-photon ionization transition amplitude is given by ([19–21])

$$T_q(i\rightarrow f)=\sum_m\frac{\langle f|D_q|m\rangle\langle m|D_q|i\rangle}{E_i+\omega-E_m}. \tag{4}$$

Here i, m, and f denote initial, intermediate, and final states; D_q is the electric dipole operator; E_i and E_m are energies of the initial and intermediate states, respectively; and the sum over m abbreviates summation over the discrete and integration over continuum states.

In the LOPT, the following transitions are allowed:

$$5p^6 \dashrightarrow 5p^5_{j_c}\varepsilon'\ell' j' \dashrightarrow 5p^5_{j_c}\varepsilon\ell j, \tag{Ia}$$

$$5s^25p^6 \dashrightarrow 5s^15p^6\varepsilon\ell j \dashrightarrow 5s^25p^5_{j_c}\,\varepsilon\ell j. \tag{Ib}$$

Here the transitions to the $5p^5\varepsilon p$ states proceed via the interfering $5p^5\varepsilon' s$ and $5p^5\varepsilon' d$ intermediate states, whereas the transitions to the $5p^5\varepsilon f$ states proceed via the $5p^5\varepsilon' d$ intermediate states only.

The electron correlations can be expressed as complementary amplitudes including matrix elements of the Coulomb interaction. Those amplitudes are of the next order of PT and describe all possible one- and two-electron excitations allowed by the selection rules in the initial, final, and intermediate states. Here we classified those correlation amplitudes in accord with [15] and [8].

Intermediate-state interchannel correlation:

$$5p^6 \dashrightarrow 5p^5_{j_c}\varepsilon''\ell'' \rightarrow 5p^5_{j_c}\varepsilon'\ell' \dashrightarrow 5p^5_{j_c}\varepsilon\ell j. \tag{II}$$

Ground-state correlations:

$$5p^6 \rightarrow 5p^4\varepsilon'\ell'\varepsilon''\ell'' \dashrightarrow 5p^5_{j_c}\varepsilon'\ell' \dashrightarrow 5p^5_{j_c}\varepsilon\ell j, \tag{IIIa}$$

$$5p^6 \rightarrow 5p^4\varepsilon'\ell'\varepsilon''\ell'' \dashrightarrow 5p^4\varepsilon\ell j\varepsilon''\ell'' \dashrightarrow 5p^5_{j_c}\varepsilon\ell j, \tag{IIIb}$$

$$5p^6 \rightarrow 5p^4\varepsilon\ell j\varepsilon''\ell'' \dashrightarrow 5p^4\varepsilon\ell j\varepsilon'\ell' \dashrightarrow 5p^5_{j_c}\varepsilon\ell j. \tag{IIIc}$$

Intermediate-state shake-up correlation:

$$5p^6 \dashrightarrow 5p^5_{j_c'}\varepsilon'\ell' \rightarrow 5p^4\varepsilon\ell j\varepsilon'\ell' \dashrightarrow 5p^5_{j_c}\varepsilon\ell j. \tag{IV}$$

Intermediate-state electron scattering correlation:

$$5p^6 \dashrightarrow 5p^5_{j_c'}\varepsilon'\ell' \rightarrow 5p^4\varepsilon\ell j\varepsilon''\ell'' \dashrightarrow 5p^5_{j_c}\varepsilon\ell j. \tag{V}$$

Final-state electron scattering correlations:

$$5p^6 \dashrightarrow 5p^5_{j_c'}\varepsilon'\ell' \dashrightarrow 5p^4\varepsilon'\ell'\varepsilon''\ell'' \rightarrow 5p^5_{j_c}\varepsilon\ell j, \tag{VIa}$$

$$5p^6 \dashrightarrow 5p^5_{j_c'}\varepsilon''\ell'' \dashrightarrow 5p^4\varepsilon'\ell'\varepsilon''\ell'' \rightarrow 5p^5_{j_c}\varepsilon\ell j. \tag{VIb}$$

In all schemes (I)–(VI) dashed and solid arrows denote electric dipole interaction and Coulomb interaction, respectively. We note that since two electrons are involved in the Coulomb interaction, the total angular momentum of the ionic core j_c' in the intermediate state in processes (II) and (IV)–(VI) could differ from that in the final state, j_c.

The general expression of the transition amplitude (4) for, e.g., the (Ia) process, is as follows:

$$T_q\left(5p^6 \to 5p_{j_c}^5 \varepsilon\ell j\right) = \sum_{\varepsilon'>F}\sum_{\ell'} \frac{\left\langle 5p_{j_c}^5 \varepsilon\ell j \middle| D_q \middle| 5p_{j_c}^5 \varepsilon'\ell' \right\rangle \left\langle 5p_{j_c}^5 \varepsilon'\ell' \middle| D_q \middle| 5p^6 \right\rangle}{\omega - E^{(i)}_{5p_{j_c}} - \varepsilon'}, \tag{5}$$

where $E^{(i)}_{5p_{j_c}}$ is the ionization potential of the $5p_{j_c}$ electron.

As in our previous work [8], we applied experimental [18] values of the ionization potentials ($E^{(i)}_{5p_{3/2}} = 0.8915$ Ry and $E^{(i)}_{5p_{1/2}} = 0.9875$ Ry) in the calculation of the energy denominators of the transition amplitudes. The double-ionization potential of the $5p$ shell, $E^{(i)}_{5p^2(^3P_2)} = 2.4330$ Ry, was also taken from [18].

Applying the method of [22], the expressions (5) and similar expressions for the correlation amplitudes can be factorized as a product of angular and radial parts. The latter one was calculated applying the CF technique which is described below. For the convenience of the discussion we present the two-photon transition amplitude $T_{q,\omega}(j_c,\ell,j,J)$ as a sum of the LOPT processes (Ia) and (Ib) and the correlation processes (II)–(VI):

$$T_{q,\omega}(j_c,\ell,j,J) = T^{(\mathrm{Ia})}_{q,\omega}(j_c,\ell,j,J) + T^{(\mathrm{Ib})}_{q,\omega}(j_c,\ell,j,J) + \sum_{(\mathrm{corr})} T^{(\mathrm{corr})}_{q,\omega}(j_c,\ell,j,J). \tag{6}$$

A. The LOPT process (Ia)

In one-electron approximation the two-photon LOPT transition amplitude (Ia) is expressed as a product of two parts describing the geometry (angular, f_q) and the dynamics (radial, t_ω) of the photoionization:

$$T^{(\mathrm{Ia})}_{q,\omega}(j_c,\ell,j,J) = \sum_{\ell'} f_q(j_c,\ell,j,J,\ell') t^{(\mathrm{Ia})}_\omega(j_c,\ell,j,J,\ell'). \tag{7}$$

The geometrical factors are

$$f_q(j_c,\ell,j,J,\ell') = (-1)^{3/2+j+J}([j_c][j][J])^{1/2} \times \begin{pmatrix} J & 1 & 1 \\ -2q & q & q \end{pmatrix} \begin{Bmatrix} \ell & j & 1/2 \\ j_c & 1 & J \end{Bmatrix} \times \begin{Bmatrix} \ell & J & 1 \\ 1 & \ell' & 1 \end{Bmatrix} \times (\ell\|C^{(1)}\|\ell')(\ell'\|C^{(1)}\|1), \tag{8}$$

where $(\ell\|C^{(1)}\|\ell')$ is a submatrix element of the spherical function in the standard phase system [22]; $[x] \equiv 2x+1$. The quantities in parentheses and in curly brackets are $3j$ and $6j$ symbols, respectively. The numerical values of f_q are listed in Table I.

TABLE I. Geometrical factors $f_q(j_c,\ell,j,J,\ell')$ [Eq. (8)] for the case of linearly polarized incoming radiation ($q=0$). For circular polarization ($|q|=1$) the factors are $f_1(2,\ell,\ell') = \sqrt{3/2} f_0(2,\ell,\ell')$; $f_1(0,\ell,\ell') = 0$.

j_c	ℓ	j	J	ℓ'	f_0
$\frac{1}{2}$	p	$\frac{1}{2}$	0	s	$-\frac{\sqrt{2}}{9}$
$\frac{1}{2}$	p	$\frac{1}{2}$	0	d	$-\frac{2\sqrt{2}}{9}$
$\frac{3}{2}$	p	$\frac{3}{2}$	0	s	$-\frac{2}{9}$
$\frac{3}{2}$	p	$\frac{3}{2}$	0	d	$-\frac{4}{9}$
$\frac{1}{2}$	p	$\frac{3}{2}$	2	s	$-\frac{2}{9}$
$\frac{1}{2}$	p	$\frac{3}{2}$	2	d	$-\frac{2}{45}$
$\frac{3}{2}$	p	$\frac{1}{2},\frac{3}{2}$	2	s	$\frac{2}{9}$
$\frac{3}{2}$	p	$\frac{1}{2},\frac{3}{2}$	2	d	$\frac{2}{45}$
$\frac{1}{2}$	f	$\frac{5}{2}$	2	d	$\frac{2\sqrt{2}}{5\sqrt{3}}$
$\frac{3}{2}$	f	$\frac{5}{2}$	2	d	$\frac{4}{5\sqrt{21}}$
$\frac{3}{2}$	f	$\frac{7}{2}$	2	d	$\frac{4\sqrt{2}}{5\sqrt{7}}$

The radial parts of the amplitude (7) are

$$t^{(\mathrm{Ia})}_\omega(j_c,\ell,j,J,\ell') = \sum_{\varepsilon'>F} \frac{\langle\varepsilon\ell j|d|\varepsilon'\ell'\rangle\langle\varepsilon'\ell'|d|5p\rangle}{\omega - E^{(i)}_{5p_{j_c}} - \varepsilon'}, \tag{9}$$

and they are independent of the polarization of the exciting photons. Here d is the radial part of the dipole transition operator determined in the length or velocity form.

In computing $t^{(\mathrm{Ia})}_\omega(j_c,\ell,j,J,\ell')$ (9), a dependence of the radial part of the $\varepsilon\ell j$ AOs on the total momentum j was taken into account. The respective spin-orbital potential was implemented in the Pauli-Fock (PF) equation (see Sec. II C) as in [10,23,24]. The radial parts of the intermediate-state AOs $\varepsilon'\ell'$ were calculated in the potential of the $5p^5\varepsilon'\ell'$ ($^1P_1$) state.

The radial integral $\langle\varepsilon\ell j|d|\varepsilon'\ell'\rangle$ in (9) corresponds to the transition between two continua diverges. The divergency problem was solved using the CF method. This method was discussed in detail in our previous paper [8]. Here only general lines are presented.

The CF is defined as

$$\phi_{\ell'}(r) = \sum_{\varepsilon'>F} \frac{P_{\varepsilon'\ell'}(r)\langle\varepsilon'\ell'|d|5p\rangle}{\omega - E^{(i)}_{5p_{j_c}} - \varepsilon'}. \tag{10}$$

This function is calculated by solving the inhomogeneous integro-differential equation

$$\left(h_{\ell'} - \omega + E^{(i)}_{5p_{j_c}}\right)\phi_{\ell'}(r) = -dP_{5p}(r) + \sum_{n'<F} P_{n'\ell'}(r)\langle n'\ell'|d|5p\rangle, \tag{11}$$

where $h_{\ell'}$ is the relativistic PF operator for the $\varepsilon'\ell'$ AO in the configuration $5p^5\varepsilon'\ell'(^1P_1)$. Some important details of the PF approximation [24] are discussed in Sec. II C.

The electric dipole operator d entering Eq. (11) affects the $5p$ AO as $d_L P_{5p}(r) = r P_{5p}(r)$ and $d_V P_{5p}(r) = -\frac{dP_{5p}(r)}{dr} \mp \frac{\ell_{\max}}{r} P_{5p}(r)$ in the length and velocity form, respectively [$\ell_{\max} = \max(1,\ell')$; the upper and lower signs in $\mp$ correspond to signs in expression $\ell' = \ell_c \mp 1$ where $\ell_c = 1$ is the orbital momentum of the $5p$ core electron].

With the CF $\phi_{\ell'}(r)$ (10) the radial part of the transition amplitude takes on the following form:

$$t_\omega^{(\mathrm{Ia})}(j_c,\ell,j,J,\ell') = \langle \varepsilon\ell j|d|\phi_{\ell'}\rangle. \tag{12}$$

B. The correlation processes of the third order of PT

The factorized transition amplitude for the ground-state correlation process (III) is given by

$$T_{q,\omega}^{(\mathrm{corr})}(j_c,\ell,j,J) = \sum_{\ell'} f_q(j_c,\ell,j,J,\ell') \times \sum_{\ell''} t_\omega^{(\mathrm{corr})}(j_c,\ell,j,J,\ell',\ell''). \tag{13}$$

Transition amplitudes for all other correlation processes are as follows:

$$T_{q,\omega}^{(\mathrm{corr})}(j_c,\ell,j,J) = \sum_{\ell'} f_q(j_c,\ell,j,J,\ell') \sum_{j_c'} \frac{2j_c'+1}{6} \times \sum_{\ell''} t_\omega^{(\mathrm{corr})}(j_c,j_c',\ell,j,J,\ell',\ell''), \tag{14}$$

where the sum over j_c' in (14) corresponds to a nonconservation of the total angular momentum of the $5p^5$ core.

The geometrical factors f_q listed in Table I are identical for all correlation processes (II)–(VI). Calculation of $t_\omega^{(\mathrm{corr})}$ for each correlation process (II)–(VI), performed using the CF technique, was described in detail in [8]. Minor changes to this procedure included in the present work are (i) using the relativistic PF instead of the Hartree-Fock (HF) approach in [8]; and (ii) the radial parts $t_\omega^{(\mathrm{corr})}(j_c,\ell,j,J,\ell',\ell'')$ in (13) and $t_\omega^{(\mathrm{corr})}(j_c,j_c',\ell,j,J,\ell',\ell'')$ in (14) become dependent not only on the intermediate orbital angular momenta ℓ' and ℓ'' but also on the total angular momenta j_c and j_c'. The latter dependence is a consequence of using different ionization potentials $E_{5p_j}^{(i)}$ of the $5p_j$ core in the CFs calculation.

C. Calculation of single-electron wave functions

Within the PF approximation, relativistic effects are taken into account in Breit approximation resulting in the following equation for the $n\ell j$ orbital:

$$h_{n\ell j}(r)P_{n\ell j}(r) = \left(-\frac{d^2}{dr^2} + \frac{\ell(\ell+1)}{r^2} + V_{n\ell} - X_{n\ell} + H_{n\ell}^M + H_{n\ell j}^{SO} + H_{n\ell}^D\right)P_{n\ell j}(r) = \varepsilon_{n\ell j} P_{n\ell j}(r), \tag{15}$$

where $V_{n\ell}$ is the local part of the Coulomb potential, $X_{n\ell}$ is its nonlocal (exchange) part, and $H_{n\ell}^M$, $H_{n\ell j}^{SO}$, and $H_{n\ell}^D$ are mass-velocity, spin-orbit, and Darwin terms, respectively. They are

$$H_{n\ell}^M P_{n\ell j}(r) = -\frac{\alpha^2}{4}[\varepsilon_{n\ell j} - V_{n\ell}(r)]^2 P_{n\ell j}(r), \tag{16}$$

$$H_{n\ell}^D P_{n\ell j}(r) = -\frac{\alpha^2}{4}\left(1 + \frac{\alpha^2}{4}[\varepsilon_{n\ell j} - V_{n\ell}(r)]\right)^{-1} \times r\frac{dV_{n\ell}(r)}{dr}\frac{d[P_{n\ell j}(r)/r]}{dr}, \tag{17}$$

$$H_{n\ell j}^{SO} P_{n\ell j}(r) = \frac{j(j+1) - \ell(\ell+1) - s(s+1)}{2} \times \frac{\alpha^2}{2}\left[1 + \frac{\alpha^2}{2}[\varepsilon_{n\ell j} - V_{n\ell}(r)]\right]^{-1} \times \frac{1}{r}\frac{dV_{n\ell}(r)}{dr} P_{n\ell j}(r). \tag{18}$$

AOs of the Xe atomic core were computed for the ground-state configuration and remained frozen in all calculations. AOs of $5p_{1/2}$ and $5p_{3/2}$ subshells were computed with taking into account spin-orbit potential (18). The photoelectron AOs were computed in jj coupling in the $5p^5$ configuration. The $\varepsilon p_{1/2}$ and $\varepsilon p_{3/2}$ AOs were orthogonalized to $5p_{1/2}$ and $5p_{3/2}$ AOs, respectively. The CFs (10) corresponding to the intermediate states were computed for the $5p^5\varepsilon'\ell'(^1P_1)$ state.

The PF operator $h_{l'}$ in the equations for both CFs [e.g., (11)] and final-state functions (15) contains a nonlocal exchange Coulomb part and the derivative $\frac{d[P_{n\ell j}(r)/r]}{dr}$ (17). The iteration procedure for the numerical calculation of the CF does not converge at the energies close to intermediate-state resonances [19]. To overcome this problem we applied as in [8] a technique of [25] and introduced a separate function for each exchange term which eliminates the nonlocal part in the differential equation. Thereby, a single nonlocal equation has been transformed to a system of local equations which can be solved noniteratively at any energy.

A similar computational trick has been applied for the derivative in the relativistic Darwin correction (17). Introduction of the function $Z_{nlj}(r) = \frac{d[P_{nlj}(r)]}{dr}$ transforms the second-order differential equation (15) to a set of two differential equations of the first order without a derivative of the desired wave functions in the right-hand parts. Respective equations are

$$\frac{d[P_{nlj}(r)]}{dr} = Z_{nlj}(r), \tag{19}$$

$$-\frac{dZ_{nlj}(r)}{dr} = \left(-\frac{l(l+1)}{r^2} + V_{nl} - X_{nl} + H_{nl}^M + H_{nl}^{SO}\right) \times P_{nlj}(r) - \widetilde{H}_{nl}^D Z_{nlj}(r) + \varepsilon_{nlj} P_{nlj}(r), \tag{20}$$

where

$$\widetilde{H}_{nl}^D Z_{nlj}(r) = -\frac{\alpha^2}{4}\left(1 + \frac{\alpha^2}{4}[\varepsilon_{nlj} - V_{nl}(r)]\right)^{-1} \times r\frac{dV_{nl}(r)}{dr}\left(\frac{1}{r}Z_{nlj}(r) + \frac{1}{r^2}P_{nlj}(r)\right). \tag{21}$$

The noniterative numerical solution of these equations is based on the predictor-corrector Milne scheme [26].

III. TWO-PHOTON IONIZATION CROSS SECTIONS OF THE 5*p* SHELL OF XENON

In this section we discuss the present results of calculation, and compare them with the $3p$ G2PICS of Ar and with the results existing in literature. Emphasis is laid on the influence of both relativistic effects and the many-electron correlations on the computed $5p$ G2PICS of Xe.

A. Comparison of 5*p* G2PICS of Xe and 3*p* G2PICS of Ar calculated in LOPT approximation

In order to investigate the difference between two-photon ionization of Ar and Xe we calculated the partial $5p$ G2PICS of Xe in the LS-coupling scheme taking into account the LOPT (Ia) transition only. The HF orbitals were computed for the Ar case, whereas the relativistic PF orbitals were used for Xe but without taking into account spin-orbital potential. The presently computed partial G2PICS for the $np^5\varepsilon p(^1S)$ and $np^5\varepsilon p(^1D)$ ($n = 3$ for Ar and $n = 5$ for Xe) final states are depicted in the upper panel of Fig. 1 for the energies in the region of the first $np^5(n+1)s(^1P)$ intermediate resonance. Exciting photon energies calculated for this resonance in the LS-coupling scheme amount to 11.9 and 9.2 eV for Ar and Xe, respectively.

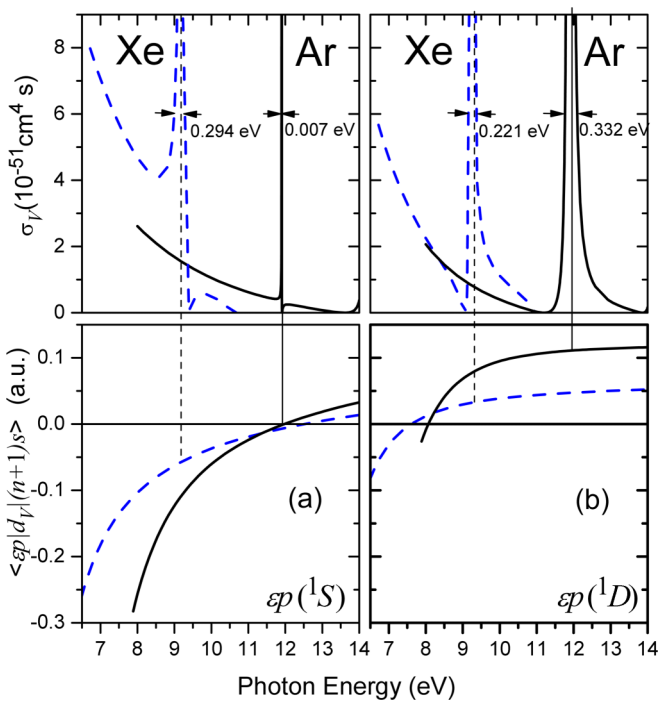

FIG. 1. The np partial G2PICS (upper panels) and respective $\langle \varepsilon p|d_V|(n+1)\,\mathrm{s}\rangle$ radial integrals (lower panels) for the transitions to the εp channels, calculated in the velocity form of dipole transition operator, LOPT, and in LS coupling for Ar ($n = 3$, solid lines) and Xe ($n = 5$, dashed lines) for the case of linearly polarized incoming radiation. We stress that here and below the abscissa axis shows the single-photon energy, thus, the energy implemented to an atom is twice larger. (a) Transitions to the $\varepsilon p(^1S)$ channel. (b) Transitions to the $\varepsilon p(^1D)$ channel. The "widths" of the resonance lines were determined at $\sigma = 6 \times 10^{-51}$ cm^4 s.

In order to have the G2PICS as a property of a target only we did not consider the width of the intermediate state m in Eq. (4) which depends on the intensity of the incoming radiation (see, e.g., [27], Eqs. (6.3)–(6.9), and comments below these equations). This consideration would result in an imaginary part of the energy E_m making the G2PICS at the resonance finite. Without the imaginary part, the G2PICS at the resonance energy is infinite and, therefore, the quantity "full width at half maximum" has no meaning. To make a quantitative comparison of the G2PICSs of Ar and Xe we introduced the "widths" determined at $\sigma = 6 \times 10^{-51}$ cm^4 s. One can see that both the "widths" and the profiles of the resonances in Ar and Xe are different.

To clarify the reason for those differences we have calculated the dependence of the radial part of the dipole matrix element $\langle \varepsilon p|d_V|(n+1)s\rangle$, describing the second step of the process (Ia), on the exciting-photon energy ω (connected with the photoelectron energy ε as $\omega = \frac{1}{2}(E^{(i)}_{np} + \varepsilon)$. The results of the calculation are depicted for Ar and Xe in the lower panel of Fig. 1. The potentials for the εp electron differ much in the $np^5\varepsilon p(^1S)$ and $np^5\varepsilon p(^1D)$ final states. The difference of the spherical parts of exchange interaction, $X_{\varepsilon p}$, for those channels is $6G^0(np\varepsilon p)$. As a consequence, the radial matrix element of the transition to the $np^5\varepsilon p(^1S)$ state has the Cooper minimum region at much larger photon energies than it has to the $np^5\varepsilon p(^1D)$ state. Therefore, the $5p^56s(^1P)$ resonance in the $5p^5\varepsilon p(^1S)$ and $5p^5\varepsilon p(^1D)$ channels lies on different sides from the Cooper minimum. The $\langle \varepsilon p|d_V|6s\rangle$ integrals have comparable values but opposite signs. Therefore, the $5p^56s(^1P)$ resonances in Xe have comparable "widths" but inverse asymmetry.

In Ar the energy of the $3p^54s(^1P)$ resonance is very close to the Cooper minimum in the $3p^5\varepsilon p(^1S)$ channel providing a narrow profile in G2PICS. In the $3p^5\varepsilon p(^1D)$ channel the position of this resonance is substantially above the Cooper minimum. Therefore, the $\langle \varepsilon p|d_V|4s\rangle$ integral is large and the respective resonance has a large "width" and the same asymmetry as in xenon.

Another interesting observation in Fig. 1 is that the threshold value of the G2PICS in Xe is three times larger than in Ar. To understand the reason for this difference we calculated the single-photon ionization cross section (PICS) of the outer np shell of both atoms because the right-hand side of Eq. (5) contains the respective transition matrix element. Frozen-core single-electron approximation and the LS-coupling scheme were used. The results are presented in Fig. 2 for the length form of the dipole transition operator. One can see that the threshold single-photon PICS of Xe is about twice larger than that for Ar. Thus, a large difference between threshold G2PICS of Xe and Ar is caused by a large difference in the density of the oscillator strengths of the single-electron np-εd transition near the np thresholds.

B. Influence of relativistic effects and core polarization on the energy positions of the $5p^5_{j_c}n\ell$ resonances

Previously, we revealed that in the case of Ar core polarization decreases the energy of the intermediate $3p^54s$ resonance by $\Delta E^{(\mathrm{CP})}_{3p^54s} = -0.27$ eV providing good agreement between theory and experiment [8]. In the case of Xe, the

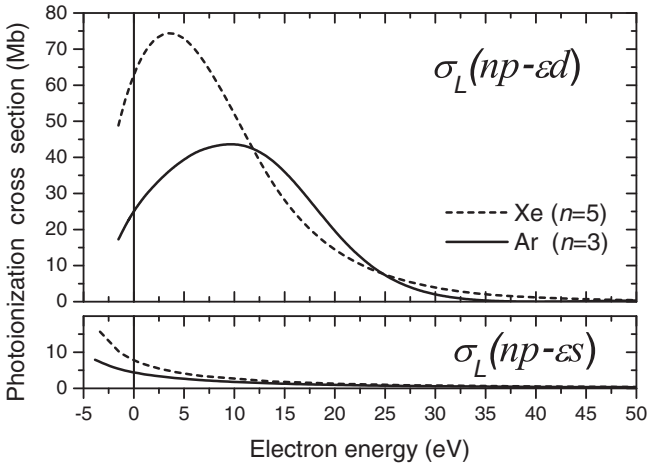

FIG. 2. Calculated partial single-photon ionization cross section of the outer np shells of Ar and Xe.

influence of core polarization is larger than in Ar. The shift of the $5p^5 6s$ resonance resulting from taking into account the core polarization potential $V^{\rm CP}(r)$ [28] is $\Delta E^{\rm (CP)}_{5p^5 6s} = -0.36$ eV. The shift of the $5p^5 6s$ resonance connected with relativistic effects is smaller than $\Delta E^{\rm (CP)}_{5p^5 6s}$ being, however, substantial: $\Delta E^{\rm (rel)}_{5p^5 6s} = -0.11$ eV. In the case of the $5p^5 5d$ resonance the influence of both effects is much smaller: $\Delta E^{\rm (CP)}_{5p^5 5d} = -0.08$ eV, $\Delta E^{\rm (rel)}_{5p^5 5d} = -0.02$ eV.

The influence of both effects on the position of the intermediate-state resonances is presented in Fig. 3. In the upper panel the extended energy region starting from the double-photon ionization threshold including the $5p^5_{3/2}6s$, $5p^5_{1/2}6s$, $5p^5_{3/2}5d$, and $5p^5_{3/2}7s$ resonances is displayed. In the lower panel the enlarged region of the closely lying $5p^5_{3/2}5d$ and $5p^5_{3/2}7s$ resonances is shown. In the top panel of Fig. 3 experimental energies of the intermediate resonances from the NIST database [18] are also shown. Notations of the resonances are labeled using the jK coupling: $6s[3/2]_1$ and $6s'[1/2]_1$ denote $5p^5_{3/2}6s[3/2]J=1$ and $5p^5_{1/2}6s[1/2]J=1$, respectively (the prime is a commonly used mark for the states with $j_c = 1/2$).

It is evident from Fig. 3 that core polarization and relativistic effects substantially improve the agreement between the computed and measured energies of the intermediate resonances. In Xe, however, the overall agreement between experiment and theory is not as good as in Ar. An additional investigation showed that this is explained by the $5p^5 5d$-$5p^5 \varepsilon d$ Coulomb interaction and s-d mixing due to the interaction of the, e.g., $6s'[1/2]_1$ and $5d[K]_1$ resonances, which are particularly strong in Xe [29] and which have not been included in the present work.

C. Results of calculation of the $5p$ G2PICS of Xe

The G2PICS computed for the $5p$ shell of Xe within the LOPT [processes (Ia) and (Ib)] are depicted in Fig. 4 in a logarithmic scale (curves PF L and PF V). In the same figure we also show the G2PICS computed with taking into account correlation amplitudes (II)–(VI) and core polarization

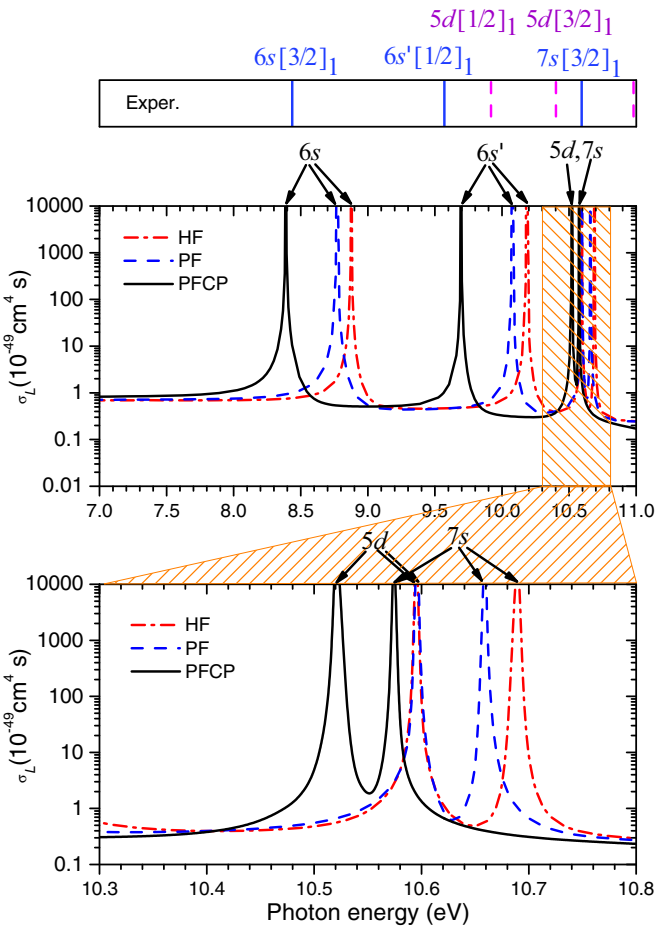

FIG. 3. The $5p$ total G2PICS of Xe computed in the nonrelativistic LOPT (HF), relativistic LOPT (PF), and with taking into account core polarization (PFCP). The length form of electric dipole operator for the linear polarization of exciting radiation was used. In the bottom panel the region of close-lying $5p^5_{3/2}5d$ and $5p^5_{3/2}7s$ resonances is presented with enlarged scale. In the top panel the experimental [18] energies of the resonances are shown.

(curves CIPFCP L and CIPFCP V). When computing cross sections CIPFCP L and CIPFCP V we accounted for some correlations of the third orders of PT by scaling the transition amplitudes (II)–(VI) with a factor 1/1.26 (see [8,10], and references therein). In the same figure we denote the only experimental G2PICS [30] by a star and the experimental energies of the intermediate $5p^5 n\ell$ resonances [18] by bars.

Taking into account the above correlations reduces the relative difference $|\sigma_L - \sigma_V|/[\frac{1}{2}(\sigma_L + \sigma_V)]$ at the threshold from 80% (PF approach) to 7.7% (CIPFCP). The latter number can be considered as a measure of accuracy of the present calculation.

In order to illustrate the influence of the intershell correlations [last two steps of the processes (V) and (VI)] on the difference between σ_L and σ_V we used the L-form data for the $5p^5_{3/2}6s(J_0=2) \to 5p^5_{3/2}\varepsilon p_{3/2}(J=3)$ transition from our earlier work [24] together with the calculation performed in the present paper in the V form. The main correlations which were taken into account in [24] are the intershell correlations. The importance of these correlations is illustrated in Fig. 5

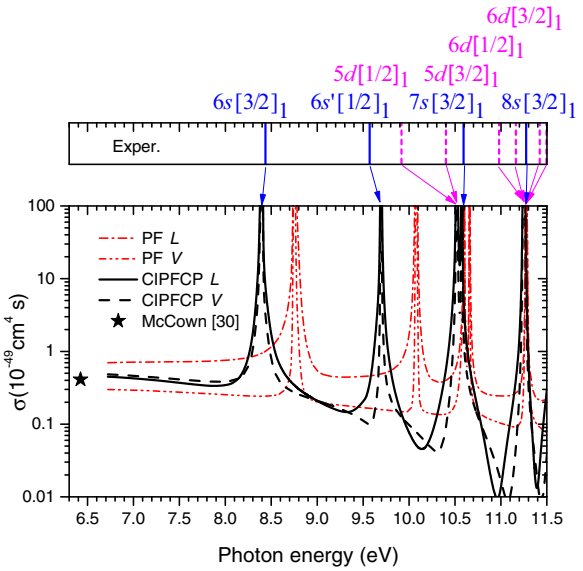

FIG. 4. The $5p$ total G2PICS of Xe in length (L) and velocity (V) form for linearly polarized incoming radiation calculated in relativistic LOPT approximation (PF) and with taking into account correlation and core-polarization effects (CIPFCP). Experimental point: [30]. Top panel: experimental [18] energies of the resonances.

where transition amplitudes for this process computed with (CIPF) and without (PF) many-electron correlations are depicted. We would like to note that the resulting "many-electron" amplitude neither coincides with the "single-electron" amplitude in length form nor in velocity form. The importance of this statement is connected with long-term discussion on what form of the electric dipole operator is better for the calculations (see, e.g., works [16,31,32]).

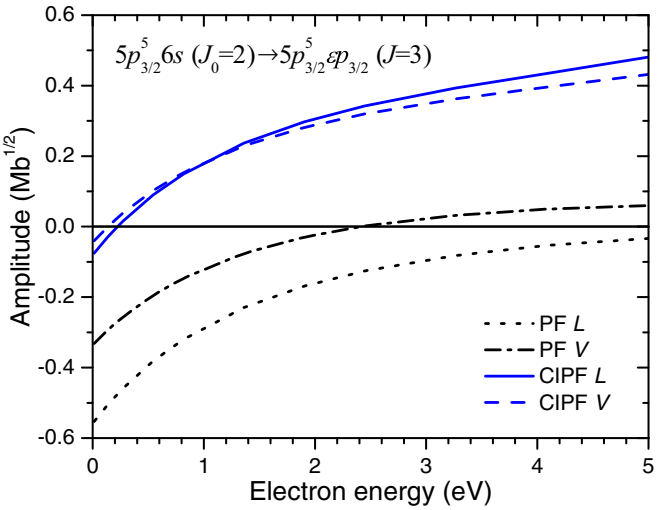

FIG. 5. Partial photoionization amplitudes of the $5p^5_{3/2}6s(J_0 = 2)$ state of Xe* calculated in a single-electron relativistic Pauli-Fock approximation (PF) and with taking into account many-electron correlations (CIPF) in the length (L) and velocity (V) form of the electric dipole operator.

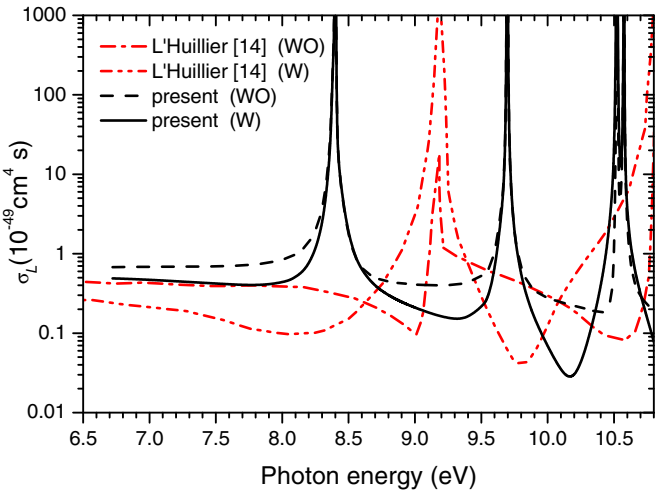

FIG. 6. Comparison between the $5p$ total G2PICS of Xe computed by L'Huillier and Wendin [14] and in the present paper with (W) and without (WO) "nonlinear screening." Linearly polarized exciting photons and the length form of the transition operator were used in both calculations.

A linear extrapolation of the CIPFCP cross section to the region below 6.72 eV shows good agreement between computed and measured [30] G2PICSs (see Fig. 4).

D. Comparison with other calculations

The importance of the final-state electron scattering correlations (V) and (VI) in computing the $5p$ two-photon ionization of Xe has been pointed out by L'Huillier and Wendin [14] who called these correlations "nonlinear screening." The $5p$ total G2PICS computed in [14] with (W) and without (WO) nonlinear screening are compared with the corresponding present cross sections in Fig. 6. In order to provide consistency of comparison between data [14] and our data we excluded the correlation (IV) from our calculation, which was also not taken into account in [14]. An essential difference in the positions of the intermediate-state resonances is seen from Fig. 6. It is because the nonrelativistic HF approach was applied in [14] and, therefore, the $6s$ and $6s'$ resonances have equal energy.

Our calculation confirms, in general, the statement of L'Huillier and Wendin [14] that the non-linear screening decreases the G2PICS. However, in our case this decrease is less pronounced as in [14]: at a photon energy of 8 eV the nonlinear screening correlation decreases the G2PICS by a factor of 4 in [14], whereas in the present calculation the respective factor equals only to 2. The difference could be connected with the different set of AOs (relativistic with core polarization PFCP in our case and nonrelativistic HF in [14]).

Pan *et al.* [15] have revealed the importance of the intermediate-state shake-up correlation (IV) in computing the G2PICS of Ar. Taking into account this correlation significantly changes cross sections and pulls together the $3p$ G2PICS of Ar computed in length and velocity gauges. In the case of Xe, the shake-up correlation (IV) has a similar influence on the $5p$ G2PICS. One can recognize this from Fig. 7, where partial G2PICSs for the transition to the $5p^5_{3/2}\varepsilon p_{3/2}(J = 0)$ channel, computed in the present paper, are

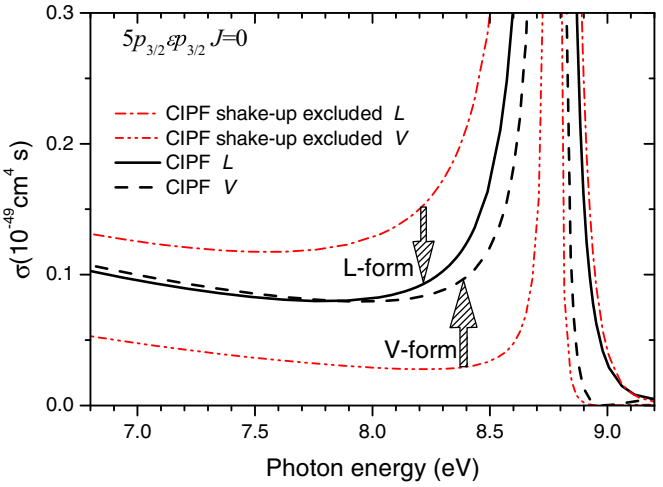

FIG. 7. Partial G2PICS for the transition to the $5p^5_{3/2}\varepsilon p_{3/2}(J = 0)$ channel, computed for the linearly polarized incoming radiation without (CIPF shake-up excluded) and with (CIPF) accounting for shake-up correlation (IV).

depicted. Calculation was performed with (CIPF) and without (CIPF shake-up excluded) shake-up correlation (IV).

The Xe $5p$ G2PICSs computed in the present paper for linearly polarized exciting radiation are compared with G2PICS computed in [13,16] in Fig. 8. Fink and Johnson [16] performed a calculation using a fairly precise relativistic TDDF method which, as was mentioned by the authors, is closely related to the RRPA. One can see that our G2PICSs are in close agreement with the G2PICS obtained in [16] in the energy range between the two-photon $5p_{1/2}$ threshold and the lowest $5p^5_{3/2}6s$ resonance. In the close-to-resonance region the iterative procedure of solving the TDDF equations converges poorly [16] and above the $5p^5_{3/2}6s$ resonance it is difficult to obtain convergence at all [16]. Figure 8 shows that, indeed, both the width of the resonance and the absolute G2PICS differ significantly from quantities computed in the present paper.

The earlier calculations of the Xe $5p$ G2PICSs [11,13] have been performed with approximate atomic orbitals and, therefore, there is a strong difference between them and both our calculation and the calculation [16] even in the off-resonance region. McGuire [11] has used a straight-line approximation of the nonrelativistic Hermann-Skillman potential [12] and the Green's function technique in order to compute G2PICS of all rare gases. The energies of intermediate resonances were taken from experiment. This approximation overestimated the G2PICS at the off-resonance region by a factor of about 4 (see lower panel of Fig. 8). This result can be connected with the fact that the local density approximation used in [12] results in more localized near-threshold continuum orbitals and, therefore, in too large cross sections.

Gangopadhyay *et al.* [13] applied in their calculation the MQDT approximation taking experimental energies of intermediate resonances, as well. The computed cross section is about a factor of 3 smaller than ours (see upper panel of Fig. 8). The character of disagreement between the MQDT and CIPFCP $5p$ G2PICS allows us to assume that the MQDT underestimates the density of the oscillator strengths

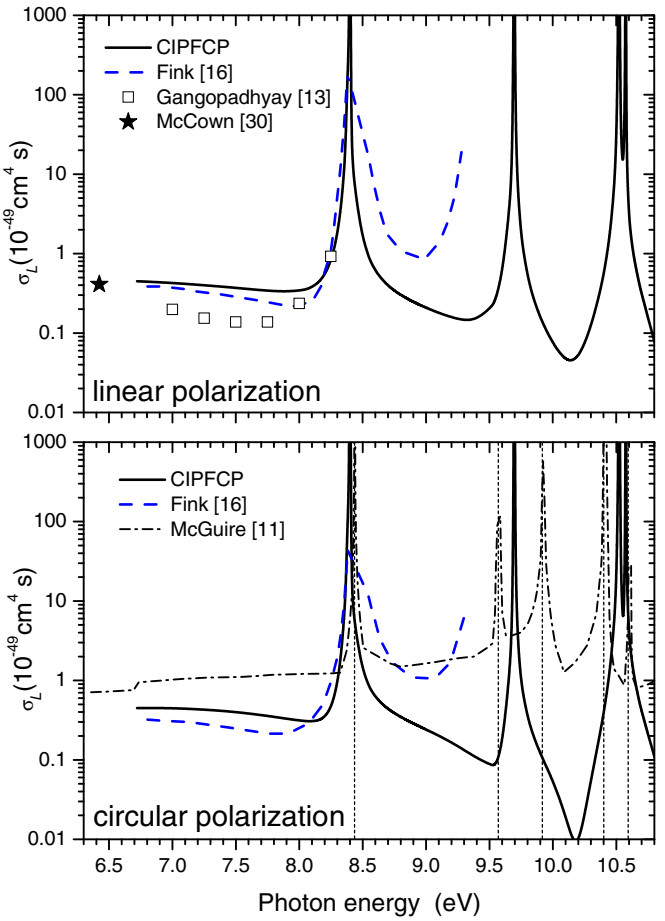

FIG. 8. The $5p$ total G2PICS of Xe calculated in the length form of the electric dipole operator for the linear (upper panel) and circular (lower panel) polarizations of incoming radiation in the present paper (CIPFCP), in [11], in [13], and in [16]. Experimental data: [30]. Experimental energies [18] of the intermediate resonances are shown as vertical lines.

of the single-electron np-$\varepsilon\ell$ transition for heavy atoms. The calculation published in [13] results also in approximately equal G2PICSs of $5p^5_{3/2}$ and $5p^5_{1/2}$ levels. However, as follows from Table I, the summed $5p^5_{3/2}$ G2PICS should be twice larger than the summed $5p^5_{1/2}$ G2PICS, which was also confirmed by the calculation in [16].

IV. ANGULAR DISTRIBUTION OF PHOTOELECTRONS

The expression for the differential G2PICS is as follows:

$$\frac{d\sigma_q(\omega)}{d\Omega} = \frac{\sigma_q(\omega)}{4\pi}\left[1 + \beta^q_2(\omega)P_2(\cos\theta) + \beta^q_4(\omega)P_4(\cos\theta)\right], \quad (22)$$

where β^q_λ are angular-distribution parameters for photoelectrons, P_λ is the Legendre polynomial, and θ is the angle between the momentum of photoelectron and electric field vectors for the linearly polarized incident radiation ($q = 0$) or between the momentum of photoelectron and the direction

of propagation vectors of the circularly polarized incoming radiation ($q = \pm 1$).

The formula for the photoelectron angular-distribution parameters was obtained using a method similar to that described in [8] but for the case of jj coupling:

$$\beta_\lambda^q(\omega) = \frac{8\pi^3 \alpha a_0^5}{c\sigma_q(\omega)} \omega^{\pm 2} \sum_{\ell\ell' jj' JJ'} (-1)^{J+2q+1/2-J'-j_c} \times [\lambda]([\ell][\ell'][j][j'][J][J'])^{1/2} e^{i(\delta_{\ell j}-\delta_{\ell' j'})} \times \begin{pmatrix} \lambda & \ell & \ell' \\ 0 & 0 & 0 \end{pmatrix} \begin{pmatrix} \lambda & J & J' \\ 0 & -2q & 2q \end{pmatrix} \times \begin{Bmatrix} \lambda & j & j' \\ 1/2 & \ell' & \ell \end{Bmatrix} \begin{Bmatrix} \lambda & J & J' \\ j_c & j' & j \end{Bmatrix} \times T_{q,\omega}(j_c,\ell,j,J) T^*_{q,\omega}(j_c,\ell',j',J'). \quad (23)$$

As in the paper [8] the standard phase system [22] for the spherical harmonics was used in Eq. (23). In addition, in Eq. (23) we took explicitly into account that the projection of the total angular momentum M_J of the final state $5p^5\varepsilon\ell j(J)$ after the absorption of two photons with polarization q equals to $2q$.

The parameter β_2^0 of the angular distribution of photoelectrons in two-photon ionization of the $5p$ shell of Xe calculated in the LOPT approximation [the processes (Ia) and (Ib) were taken into account only] is presented in Fig. 9(a) for the case of linearly polarized incoming radiation. The computed energies of the intermediate resonances are plotted as dashed lines.

The β_λ^0 parameters computed after taking into account many-electron correlations [processes (II)–(VI)] and core polarization are depicted in Figs. 9(b) and 9(c). In the case of circularly polarized incoming radiation the $\beta_2^{\pm 1}$ and $\beta_4^{\pm 1}$ parameters are connected by the simple expression $\beta_2^{\pm 1} = -1 - \beta_4^{\pm 1}$. Therefore, we show in Fig. 9(d) only the $\beta_4^{\pm 1}$ parameter.

One can recognize that electron correlations (including core polarization) improve agreement between β_2^0 parameters at the two-photon ionization threshold region (up to 8.5 eV of the exciting photon energy) only. At larger energies there exists a quite substantial difference between the β_λ^q parameters computed in length and velocity forms. These disagreements indicate that the angular-distribution parameters are more sensitive to the accuracy of calculation of many-electron effects and indicate the necessity of taking into account higher orders of PT corrections.

V. CONCLUSIONS

In the current work the influence of the relativistic effects and many-electron correlations including core polarization on the two-photon ionization of the $5p$ shell of Xe was studied. The two-photon transition amplitudes were calculated using the noniterative correlation function method, developed earlier in nonrelativistic approximation [8] and extended here for the relativistic case. Relativistic effects mainly shift energies of the intermediate $5p_{j_c}^5 ns$ resonances toward the threshold. A similar trend can be seen when core polarization is included in the calculations. Both effects together improve considerably the agreement between calculated and measured resonance energies. As there is only one experimental data point for this process a meaningful comparison to experiment for the full investigated exciting-photon energy range cannot be carried out this time. Therefore we checked the consistency between calculations using the length and the velocity form of the dipole operator. It turned out that the calculated cross sections are close to each other only when electron correlations are included in the calculations. Additionally the calculated cross sections are 22% higher when core polarization is included in the calculations. Finally, the angular-distribution parameters of the outgoing photoelectrons have been calculated. We intend to stimulate with the present theoretical work more experiments to benchmark the present calculations and to pin down those effects being dominant for this two-photon photoionization process.

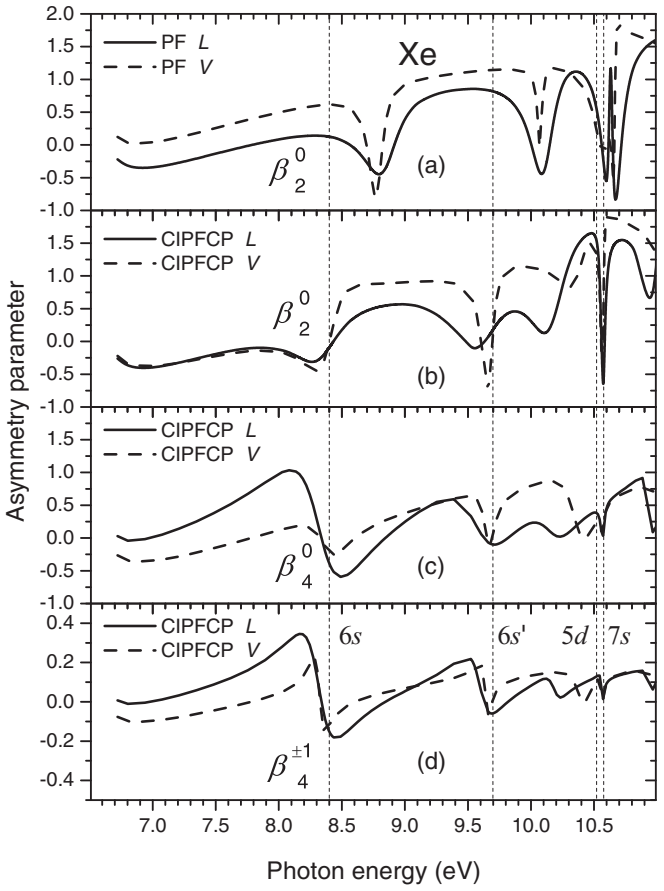

FIG. 9. Angular-distribution parameters β_λ^q for photoelectrons computed for the $5p$ two-photon ionization of Xe in the length (L) and velocity (V) form in relativistic LOPT approximation (PF) and with taking into account correlation and core-polarization effects (CIPFCP). Energies of the intermediate resonances calculated in CIPFCP approximation are shown as vertical lines.

ACKNOWLEDGMENTS

This work was supported by the Hessen State Initiative for the Development of Scientific and Economic Excellence (LOEWE) in the LOEWE-Focus project ELCH. Financial support from Deutsche Forschungsgemeinshaft (DFG Project No DE2366/1-1) is gratefully acknowledged. I.D.P., B.M.L.,

and V.L.S. would like to thank the Institute of Physics, University of Kassel for the hospitality extended to them. V.L.S. appreciates the support from Southern Federal University within the inner project No. 3.6105.2017/8.9. I.D.P. and B.M.L. appreciate the support from Russian Foundation for Basic Research (RFBR (Russia) Grant No. 16-02-00666A).

[1] W. Ackermann, G. Asova, V. Ayvazyan, and A. Azima, Nat. Photonics **1**, 336 (2007).
[2] T. Shintake, H. Tanaka, T. Hara, and T. Tanaka, Nat. Photonics **2**, 555 (2008).
[3] P. Emma, R. Akre, J. Arthur, and R. Bionta, Nat. Photonics **4**, 641 (2010).
[4] T. Ishikawa, H. Aoyagi, T. Asaka, and Y. Asano, Nat. Photonics **6**, 540 (2012).
[5] A. A. Sorokin, S. V. Bobashev, T. Feigl, K. Tiedtke, H. Wabnitz, and M. Richter, Phys. Rev. Lett. **99**, 213002 (2007).
[6] M. G. Makris, P. Lambropoulos, and A. Mihelič, Phys. Rev. Lett. **102**, 033002 (2009).
[7] M. Richter, M. Y. Amusia, S. V. Bobashev, T. Feigl, P. N. Juranić, M. Martins, A. A. Sorokin, and K. Tiedtke, Phys. Rev. Lett. **102**, 163002 (2009).
[8] I. D. Petrov, B. M. Lagutin, V. L. Sukhorukov, A. Knie, and A. Ehresmann, Phys. Rev. A **93**, 033408 (2016).
[9] P. Lambropoulos, in *Advances in Atomic and Molecular Physics*, edited by D. Bates and B. Bederson (Academic, New York, 1976), Vol. 12, pp. 87–164.
[10] V. L. Sukhorukov, I. D. Petrov, M. Schäfer, F. Merkt, M.-W. Ruf, and H. Hotop, J. Phys. B: At., Mol. Opt. Phys. **45**, 092001 (2012), Topical Review.
[11] E. J. McGuire, Phys. Rev. A **24**, 835 (1981).
[12] F. Herman and S. Skillman, *Atomic Structure Calculations* (Prentice-Hall, Englewood Cliffs, 1963).
[13] P. Gangopadhyay, X. Tang, P. Lambropoulos, and R. Shakeshaft, Phys. Rev. A **34**, 2998 (1986).
[14] A. L'Huillier and G. Wendin, Phys. Rev. A **36**, 4747 (1987).
[15] C. Pan, B. Gao, and A. F. Starace, Phys. Rev. A **41**, 6271 (1990).
[16] M. G. J. Fink and W. R. Johnson, Phys. Rev. A **42**, 3801 (1990).
[17] G. Mainfray and G. Manus, Rep. Prog. Phys. **54**, 1333 (1991).
[18] A. Kramida, Y. Ralchenko, J. Reader, and NIST ASD Team, *NIST Atomic Spectra Database (version 5.2)[Online]* (National Institute of Standards and Technology, Gaithersburg, MD, 2014), http://physics.nist.gov/asd.
[19] A. F. Starace and T.-F. Jiang, Phys. Rev. A **36**, 1705 (1987).
[20] T. N. Chang and R. T. Poe, J. Phys. B: At. Mol. Phys. **9**, L311 (1976).
[21] T. N. Chang and R. T. Poe, Phys. Rev. A **16**, 606 (1977).
[22] A. P. Jucys and A. J. Savukinas, *Mathematical Foundation of the Atomic Theory*, 1st ed. (Mintis, Vilnius, 1973) (in Russian).
[23] B. M. Lagutin, I. D. Petrov, V. L. Sukhorukov, S. B. Whitfeld, B. Langer, J. Viefhaus, R. Wehlitz, N. Berrah, W. Mahler, and U. Becker, J. Phys. B: At., Mol. Opt. Phys. **29**, 937 (1996).
[24] R. Kau, I. D. Petrov, V. L. Sukhorukov, and H. Hotop, Z. Phys. D **39**, 267 (1997).
[25] K. Smith, R. J. W. Henry, and P. G. Burke, Phys. Rev. **147**, 21 (1966).
[26] J. C. Butcher, *Numerical Methods for Ordinary Differential Equations* (Wiley, New York, 2003), pp. 1–440.
[27] P. Lambropoulos, Phys. Rev. A **9**, 1992 (1974).
[28] I. D. Petrov, V. L. Sukhorukov, and H. Hotop, J. Phys. B: At., Mol. Opt. Phys. **32**, 973 (1999).
[29] R. Kau, I. D. Petrov, V. L. Sukhorukov, and H. Hotop, J. Phys. B: At., Mol. Opt. Phys. **31**, 1011 (1998).
[30] A. W. McCown, M. N. Ediger, and J. G. Eden, Phys. Rev. A **26**, 3318 (1982).
[31] H. W. van der Hart, M. A. Lysaght, and P. G. Burke, Phys. Rev. A **76**, 043405 (2007).
[32] S. Hutchinson, M. A. Lysaght, and H. W. van der Hart, J. Phys. B **43**, 095603 (2010).